Yu She[1]
Department of Mechanical and Aerospace Engineering,
The Ohio State University,
Columbus, OH 43210
e-mail: yushe@mit.edu

Siyang Song
Walker Department of Mechanical Engineering,
University of Texas at Austin,
Austin, TX 78712
e-mail: sysong@utexas.edu

Hai-Jun Su
Professor
Fellow ASME
Department of Mechanical and Aerospace Engineering,
The Ohio State University,
Columbus, OH 43210
e-mail: su.298@osu.edu

Junmin Wang
Professor
Fellow ASME
Walker Department of Mechanical Engineering,
University of Texas at Austin,
Austin, TX 78712
e-mail: JWang@austin.utexas.edu

A Comparative Study on the Effect of Mechanical Compliance for a Safe Physical Human–Robot Interaction

In this paper, we study the effects of mechanical compliance on safety in physical human–robot interaction (pHRI). More specifically, we compare the effect of joint compliance and link compliance on the impact force assuming a contact occurred between a robot and a human head. We first establish pHRI system models that are composed of robot dynamics, an impact contact model, and head dynamics. These models are validated by Simscape simulation. By comparing impact results with a robotic arm made of a compliant link (CL) and compliant joint (CJ), we conclude that the CL design produces a smaller maximum impact force given the same lateral stiffness as well as other physical and geometric parameters. Furthermore, we compare the variable stiffness joint (VSJ) with the variable stiffness link (VSL) for various actuation parameters and design parameters. While decreasing stiffness of CJs cannot effectively reduce the maximum impact force, CL design is more effective in reducing impact force by varying the link stiffness. We conclude that the CL design potentially outperforms the CJ design in addressing safety in pHRI and can be used as a promising alternative solution to address the safety constraints in pHRI.
[DOI: 10.1115/1.4046068]

Keywords: compliant mechanisms, design theory and methodology, variable stiffness design, robot design, robotic systems

1 Introduction

In recent years, increasing interest of researchers has been drawn to the collaborative robots or co-robots, which are intentionally designed for physical interaction with human beings. Co-robots have been widely used in variable applications, including automotive industries [1], surgical assistance [2], homes/offices service [3], and so on. Unlike traditional industrial robots that are kept separated from humans to ensure safety, co-robots are designed to physically interact with humans in a shared workspace. However, safety has been a major concern that limits their applications.

Typical solutions to address safety concerns may include the sensor-based approach and mechanical design-based method. A classic application of the sensor-based method is active impedance control, which enables actuators to mimic the impedance behavior with software control algorithms [4–6]. The advantage of the active impedance control is that the algorithm can adapt to both damping and stiffness modulation with an infinite range in theory while the drawback of the impedance controller is that it is fairly complex and requires precise dynamic models. In addition, the sensor-based solution may rely heavily on a fully equipped and sensorized computer environment with robust control algorithms. Extensive studies on specific sensors, such as tactile/infrared/ultrasonic/vision sensors, can be found in the literature [7–10] for collision detection and avoidance. With the fusion of data from those sensors, a sensorized description of the environment could be established, which enables artificial intelligence [11] and advanced control algorithms [12] to play roles to address the safety issues for pHRI. The sensor-based approach with control may be one of the most proven methods for addressing the safety issue [13], but it addresses safety at the cost of extensive redundant sensors and complex fusion algorithms.

As a complementary solution, the mechanical design-based approach may offer an alternative method to address the safety issue for pHRI. Mechanical compliance introduced to robots is not subject to failure/saturation/drifting of sensors, hence guarantee intrinsic safety. Joint compliance and link compliance are two typical representatives to introduce mechanical compliance to robots. Authors in Refs. [14–17] introduced mechanical compliance to robot joints and developed compliant nonlinear actuators with optimal controllers for intrinsic safety. The variable stiffness actuator (VSA) I in Ref. [18] can change its stiffness rapidly and continuously by releasing and stretching a timing transmission belt, while the VSA II in Ref. [19] is developed via four-bar mechanisms with a nonlinear relation of torque and displacement. Chen et al. [20] exploited the optimal control of the compliant actuator to maximize the operation joint velocity. Germany Aerospace Center (DLR) developed a variable stiffness joint (VSJ) for an anthropomorphic arm in Refs. [21–23]. The VSJ is designed based on floating springs and superimposed cam mechanisms. In addition to the application of torque sensing, the VSJ can be used as a mechanical buffer to reduce maximum torques for system safety, and the passive compliance may have the potential to absorb energy from an impact for human safety. Zinn et al. [24] studied the joint compliance and designed a distributed macro-mini actuation with inherent safety for the human-friendly robot that maintains the high-frequency torque capability. Haddadin et al. [25,26] investigated the joint compliance for intrinsic safety and observed that the joint compliance may decouple the motor inertia from the link inertia via conducting extensive experimental tests, and hence reducing joint compliance may not necessarily reduce the impact force. More studies related to the VSJ can be found but are not limited to Refs. [27–31].

While extensive research has been conducted on the joint compliance, relatively less research has been investigated on the link

[1]Present address: Computer Science and Artificial Intelligence Laboratory, Massachusetts Institute of Technology, Cambridge, MA 02139.

Contributed by the Mechanisms and Robotics Committee of ASME for publication in the Journal of Mechanical Design. Manuscript received May 14, 2019; final manuscript received January 4, 2020; published online January 21, 2020. Assoc. Editor: Joo H. Kim.

compliance. Park et al. [32–34] developed a safe link mechanism that can switch its stiffness from high to low depending on the external collision force. Authors in Refs. [35,36] developed a similar mechanical fuse on robotic links to guarantee safety for pHRI. However, all of these designs are bimodal, i.e., the stiffness is not continuously tunable but can be switched between low and high modes. Recently, the variable stiffness link (VSL) has received increasing attention as an alternative inherently safe solution. Stilli et al. [37] explored a stiffness controllable soft manipulator via combining pneumatic and tendon-driven actuators. Later, they developed a VSL made of an airtight chamber by flexible and high-strain resistant combination of a plastic meshed silicone wall [38]. The silicone chamber is rigid with high-pressure air but becomes soft by reducing the air pressure. She et al. [39,40] developed a passive VSL via shape optimization for inherently safe pHRI. She et al. [41–43] also proposed a continuously tunable stiffness robotic link actuated by a pair of four-bar linkages. The mechanism is able to morph the side beams, tune the second moment of inertia of the side beams, and change the lateral stiffness of the robotic link.

Both the VSJ and VSL introduce inherent compliance to safe pHRI. Another mechanical-based approach is by introducing inherent damping to pHRI, which includes friction dampers [44,45], electrorheological and magnetorheological dampers [46–48], eddy current dampers [49], and fluid dynamics dampers [50]. The active damping can suppress system oscillations but would require a substantial amount of energy to accomplish highly dynamic tasks [5].

To evaluate the safety effectiveness of pHRI systems with VSJ or VSL, we must specify a safety criterion. While the head impact criterion (HIC) in Ref. [51], which originated from the automotive industry, may be one possible criterion for evaluating the safety of pHRI, it brings some ambiguities and confusions as stated in Ref. [52]. Haddadin et al. [25] conducted standardized crash tests with KUKA robots and found that the HIC and other similar criteria from the automobile industry are not appropriate to measure possible injuries for pHRI. In this study, we consider the worst-case scenarios of pHRI with biomechanical limits of bone fracture as safety criteria. Consequently, the impact force may be an appropriate indicator since it correlated with the bone fracture [53]. Notably, the condition of static force $\leq$ 150 N from ISO-10218 [54] is not considered as the threshold in this study since it is not derived from biomechanical analysis or actual human impact experiments but based on heuristics aiming to provide a human an opportunity to actively avoid dangerous situations [25]. In addition, Haddadin et al. [25] argued that the critical force of 150 N tends to be unnecessarily conservative which excessively limits the robot's performance. Therefore, the criterion presented in Refs. [55,56] and applied in Ref. [25] is considered in this work. That is, the fraction forces for the maxilla of facial bone and frontal of cranial bone, 600 N and 4000 N, respectively, are used.

In terms of the impact force model for a safe pHRI system, there are already a few simplified models based on the mass-spring-mass model in the literature. The advantage of these simplified models is that we can derive the analytical expression of the impact force. However, the simplification assumption may not necessarily reflect the actual impact condition and some crucial subtleties may not be revealed. For instance, authors in Refs. [25,52] assumed a contact model with a linear spring and derived the analytical models of the impact acceleration and impact force based on the mass-spring-mass model. However, the contact model may have high nonlinearity and depend on the material and geometry properties. Furthermore, considering the covering material of the robot and the scalp on the skull, the piecewise Hertz contact model presented in Ref. [57] is more accurate for pHRI. The second issue with the simplified models is that they cannot distinguish the joint compliance from the link compliance, which turns out to be considerably different according to our analysis.

In summary, since both VSJ and VSL can be used to address inherent safety for pHRI, it is critical to compare their performance for designing pHRI systems with safety constraints. This work extends the preliminary work by Ref. [58] and develops models of actual pHRI systems for both compliant joint (CJ) and compliant link (CL) designs, including dynamics of compliant robots (CJ or CL), the piecewise Hertz contact model, and dynamics of the dummy head. Here, we assume that the studied pHRI system has an active (rather than passive) compliance, i.e., the robot stiffness (hence the bandwidth) is controllable. For instance, the robotic arm can be controlled in a relatively stiff form at slow motions to satisfy the requirement of high positioning accuracy and can be tuned to the high compliance mode for fast motions to keep the maximum impact force below a safe threshold. It is worth noting that although the proposed strategy may work for the task of off-line motion planning, it may be challenging to apply for tasks of dynamic motion planning unless high bandwidth of stiffness tuning mechanisms is supported.

2 Problem Statement

The problem to be addressed is described as the following. Our hypothesis is that mechanical flexibility or compliance of robots offers inherent safety for humans during pHRI. Suppose an unexpected impact occurs during a pHRI, we need to assess the level of injuries to humans. The goal of this work is to evaluate the effectiveness of mechanical compliance to enhance safety in pHRI.

The specific scientific questions to be answered in this research are as follows:

(1) How do design (mass, mass ratio, and mechanical stiffness) and actuation parameters affect the maximum force during a pHRI?
(2) How effective is varying mechanical compliance to reduce the maximum impact force?
(3) Which design is more effective in reducing the maximum impact force, compliant link, or compliant joint?

3 System Modeling of Mechanical Compliance

In this section, we will develop theoretical models of a pHRI system including contact force model, robot dynamics, and dummy head dynamics. Joint compliance and link compliance will be introduced to the robot, and their dynamics will be included in the pHRI system.

3.1 The Hertz Contact Model.

We start with the contact force modeling. Let us assume an impact occurred between an impactor and a dummy head. The impactor is installed at the tip of a robot link while the dummy head is fixed at the end of a neck bone. The impactor is composed of an end-effector with covering material as shown at the left bottom of Fig. 1, and the dummy head is composed of a scalp covering a skull bone as shown at the right bottom of Fig. 1.

Assuming the materials of the contact bodies are isotropic, homogeneous, and frictionless, the contact force $f_e(\delta)$ can be calculated based on the piecewise Hertz model given in Refs. [57,59], and δ is the penetration depth of the contact surface.

3.2 A Rigid Body Link With a Compliant Joint.

Consider that the robot in the pHRI system is composed of a compliant joint, a rigid link, and the impactor as shown on the left in Fig. 2. The human head is modeled by the dummy head, a neck bone, and a neck spring as shown on the right of Fig. 2. The motor output angle is θ, and the link input angle is q, and they may not necessarily have the same value due to the joint compliance. Given an impact from the impactor to the dummy head, the neck spring deforms by an angle of ϕ. The definitions of the parameters of the pHRI system are given in Table 1. Note the biological values of the neck refer to Ref. [60].

The dynamics of the pHRI system includes two parts: (1) dynamics of the robot itself and (2) dynamics of the dummy head, written

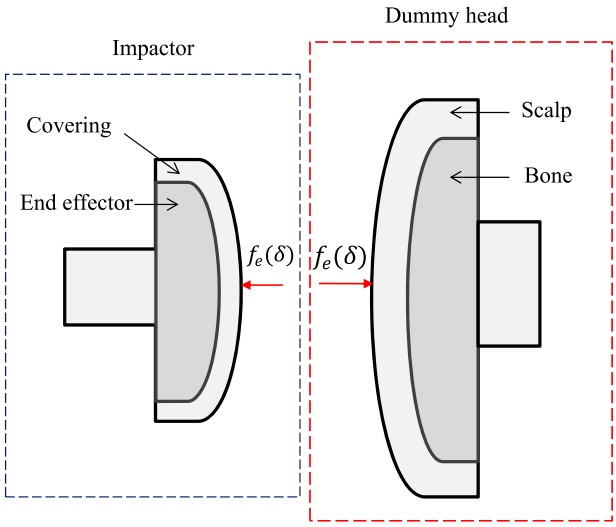

Fig. 1 The schematic diagram of the Hertz contact model

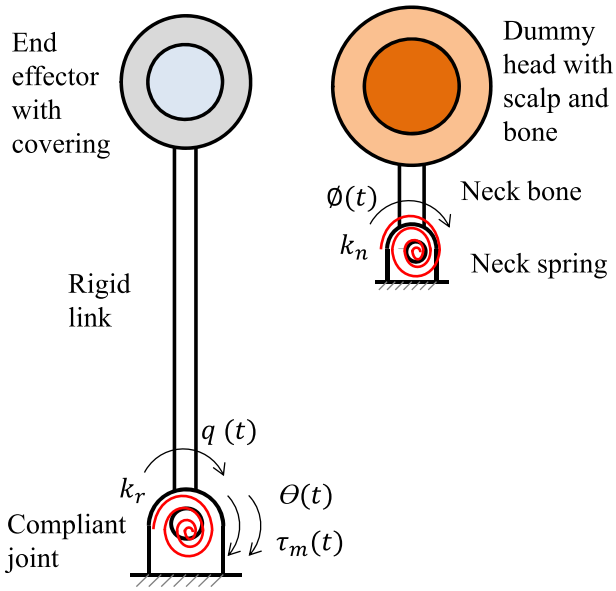

Fig. 2 Physical human–robot interaction system composed of a dummy head and a rigid link with a compliant joint

Table 1 Simulation parameters of the pHRI system

	Parameters	Symbol	Value
Motor	Damping (N s/m)	D_m	0
	Inertia (kg m^2)	I_m	4×10^{-4}
	Torque (N m)	τ_m	10
	Velocity (rad/s)	ω_0	6.25
Neck	Stiffness (N m/rad)	k_h	10
	Length (m)	l	0.147
	Mass (kg)	m_n	1
CL design	Modulus (N/m^2)	E_r	70×10^9
	Height (m)	h	0.05
	Length (m)	L	0.4
	Mass (kg)	m_r	1
	Thickness (m)	t	0.002
CJ design	Joint stiffness (N m/rad)	k_r	17.75
RR design	Joint stiffness (N m/rad)	k_r	1×10^6

as

$$\begin{cases} I_m\ddot{\theta} + \tau_k + D_m k_r^{-1}\dot{\tau}_k = \tau_m - \tau_f \\ I_r\ddot{q} + g_r(q) = \tau_k + \tau_d + \tau_{er} \\ I_h\ddot{\phi} + g_h(\phi) = \tau_h + \tau_{eh} \end{cases} \tag{1}$$

where the first two equations are dynamics of the robot with the CJ, and the third equation is the dynamics of the dummy head. In terms of the robot dynamics, τ_k, τ_d, τ_f, and τ_e are the spring torque, damping torque, friction torque, and external torque of the robot, respectively; $g_r(q)$ is the gravity term of the robot; I_r is the robot inertia that can be calculated by m_r, m_e, and m_c; I_m and D_m are the inertia and viscous damping of the motor, respectively; and J_{cj} is the Jacobian of the robot with a compliant joint and is equal to L in this case. We have

$$\begin{cases} \tau_k = k_r(\theta - q) \\ \tau_d = D_m k_r^{-1}\dot{\tau}_k = D_m(\dot{\theta} - \dot{q}) \\ \tau_e = -J_{cj}^T f_e(\delta) \end{cases} \tag{2}$$

In terms of the dummy head, I_h is the neck bone inertia that can be calculated by m_n, m_s, and m_b; $g_r(q)$ is the gravity term of the dummy head; J_h is the Jacobian of the neck bone and is equal to l in this case; τ_h and τ_{eh} are the spring torque and external torque of the dummy head, which can be calculated as follows:

$$\begin{cases} \tau_h = k_h\phi \\ \tau_{eh} = J_h^T f_e(\delta) \end{cases} \tag{3}$$

3.3 A Compliant Link With a Rigid Body Joint. Now consider a compliant robotic link that is connected to an end-effector at one end and actuated by a motor via a rigid revolute joint at the other end, as shown on the left of Fig. 3. The CL has a modulus E and a second moment of inertia I. To ensure it is comparable with the CJ design, the mass, length, and inertia of the link and parameters of the motor and the dummy head of the CL design are equivalent to those of the CJ design. In addition, the two designs should have the same lateral stiffness. Here, we consider the designs in the 2D plane and the lateral stiffness represents the task-space stiffness at the end-effector in the horizontal plane.

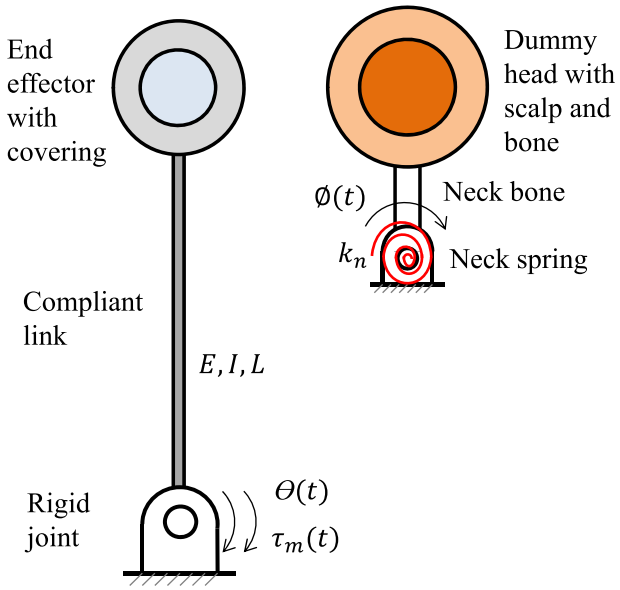

Fig. 3 Physical human–robot interaction system composed of a dummy head and a compliant link with a rigid joint

Similar to pHRI systems with a CJ, dynamics of pHRI systems with a CL also includes robot dynamics and dummy head dynamics. However, the dynamics model of compliant link is based on the assumed modes method (AMM) [61]. In summary, the dynamics of the pHRI system with CL can be mathematically formulated as

$$\begin{cases} \mathbf{M}(\mathbf{q})\ddot{\mathbf{q}} + \mathbf{N}(\mathbf{q}, \dot{\mathbf{q}}) + \mathbf{G}(\mathbf{q}) + \mathbf{K}\mathbf{q} = \tau + \tau_{er} \\ I_h\ddot{\phi} + g_h(\phi) = \tau_h + \tau_{eh} \end{cases} \tag{4}$$

where $\mathbf{M}(\mathbf{q})$ is the inertia matrix, $\mathbf{N}(\mathbf{q}, \dot{\mathbf{q}})$ contains the centrifugal and nonlinear Coriolis terms, $\mathbf{G}(\mathbf{q})$ is the gravity matrix, and $\mathbf{K}$ is the stiffness matrix. Considering the first two modes of the AMM, the generalized coordinates are $\mathbf{q} = [\theta, a_1, a_2]^T$, from which θ is the motor angle and a_1 and a_2 are modal coordinates. Given the vibration mode functions of $\varphi_1(x)$ and $\varphi_2(x)$, from which x is the position of an arbitrary point on the CL from the perspective of the floating frame, we have

$$\begin{cases} \tau = [\tau_m, 0, 0]^T \\ \tau_{er} = \mathbf{J}_{cl}^T \mathbf{F}_e(\delta) \\ \mathbf{F}_e(\delta) = [-f_e(\delta), 0]^T \\ \mathbf{J}_{cl} = \begin{bmatrix} J_{11} & -\varphi_1(L)\sin\theta & -\varphi_2(L)\sin\theta \\ J_{21} & \varphi_1(L)\cos\theta & \varphi_2(L)\cos\theta \end{bmatrix} \\ J_{11} = -L\sin\theta - (\varphi_1(L)a_1(t) + \varphi_2(L)a_2(t))\cos\theta \\ J_{21} = L\cos\theta - (\varphi_1(L)a_1(t) + \varphi_2(L)a_2(t))\sin\theta \end{cases} \tag{5}$$

where $\mathbf{J}_{cl}$ is the Jacobian of the robot with compliant link that is calculated based on AMM. The limitations of the model include compliance with the assumptions of both the hertz model and the AMM, where the later assumes that the deformation of the CL is small and can be represented by a summation of the modal shapes and a linear elasticity model.

It is worth noting that both models in above can be conveniently applied to a pHRI system with a rigid link and rigid joint (RR) by either increasing the torsion spring stiffness to infinitely (sufficiently in practice) large for the CJ configuration or increasing the robot link modulus to infinitely large for the CL configuration. In the next section, we compare three pHRI system designs based on CJ, CL, and RR by impact simulations.

3.4 Verification by Simulations. To validate the theoretical models in Eqs. (1) and (4), we established a platform for simulating the impact process of a pHRI system with CJ or CL in MATLAB Simscape Multibody based on the schematic view shown in Figs. 2 and 3. Here, we assume that the robot is operated in a horizontal plane, and friction and viscous damping are not considered. We also assume that the impact occurs with a motor torque of τ_m and an initial impact velocity of v_0. Notably, it may be reasonable assuming the negligible gravity force to design a planar robot, but the gravity should be taken into consideration to design a spatial robot. The parameters for the theoretical model and the MATLAB Simscape Multibody model are partially obtained from Refs. [35,57] and listed in Table 1.

Given those parameters in Table 1, both the CL design and the CJ design have the equivalent lateral stiffness of $k_l = 110.94$ N/m. We plot the impact force profile of these two designs compared with MATLAB Simscape Multibody simulation in Fig. 4.

It is observed that the numerical results of the theoretical models agree with those of the MATLAB Simscape Multibody models for both of the CJ and CL designs. We explored different parameter combinations, and the same results are observed, which validates the theoretical models of the pHRI system. Given the same actuation parameters, it is observed that the CL design results in a smaller impact force than that of the CJ design. In what follows, we will study a comprehensive comparison of these two designs.

4 Joint Compliance Versus Link Compliance

The pHRI theoretical models were validated in the previous section. In this section, we compare the maximum impact force of the CJ and CL designs by the pHRI simulations for various combinations of parameters including lateral stiffness, impact velocities, and motor torques.

4.1 Comparison of the Compliant Joint and Compliant Link Designs. In addition to the CL design and the CJ design, an RR design is also included in this comparison, which is obtained by modifying the CJ design with $k_r = 1 \times 10^6$ N m/rad. We plot the impact force profile of these three designs compared with MATLAB Simscape Multibody simulation in Fig. 5. It is observed that the CL design results in the smallest maximum impact force while the RR design generates the largest impact force among the three designs. The RR design generates a larger impact force compared with that of the designs with mechanical compliance. Since the RR design is not the focus in this paper, we will concentrate on the exploration of the CJ and CL design in the following sections.

Comparing the CJ with the CL design as shown in Fig. 5, it can be seen that the maximum impact force of the CL design is reduced by 12.9% when compared with that of the CJ design, and the impact force duration of the CL design is less than that of the CJ design as well. Based on this observation, we consider that the CL design may have a safer performance when compared with that of the CJ design for some situations, such as the case with the parameters given in the simulation.

In addition to the constant stiffness comparison, we would like to compare the maximum impact force of these two designs by varying stiffness. In what follows, we would like to compare the VSJ and VSL given equivalent parameters. Considering the covering material may be much lighter than that of the end-effector, here we define the mass ratio as

$$R_m = \frac{m_r}{m_e} \tag{6}$$

where m_r and m_e are the mass of the robot arm and end-effector, respectively. The actuation parameters are considered as the motor torque τ_m and the initial impact velocity v_0, and the design parameters are considered as the link stiffness k_l (effective lateral stiffness), end-effector mass m_e, and mass ratio R_m. For all other parameters except those listed in the figures, refer to Table 1.

The dynamics equations solve the impact force in terms of time $f_e(t)$, and we define F_{max} as the maximum impact force which is captured from the maximum value of each batch of simulation results of the impact force $f_e(t)$. Since the VSJ and VSL are considered here, the maximum impact force F_{max} is actually a function of the lateral stiffness k_l, i.e., $F_{max}(k_l)$. The maximum and minimal values of $F_{max}(k_l)$ are noted as max $(F_{max}(k_l))$ and min $(F_{max}(k_l))$, respectively. We then define the maximum impact force reduction R_f as

$$R_f = \frac{\max(F_{max}(k_l)) - \min(F_{max}(k_l))}{\max(F_{max}(k_l))} \times 100\% \tag{7}$$

First, we study the case of no active motor torque during the impact, i.e., $\tau_m = 0$. This is also known as "free impact." Figures 6(*a*) and 6(*b*), respectively, plot the maximum impact force F_{max} versus the lateral stiffness k_l of the VSJ and VSL without active motor torque for various impact velocity v_0. We have the following observations from these simulations:

(1) The effects of the joint stiffness on the maximum impact force for the VSJ are negligible because the joint spring has decoupled the motor and link inertia by the intrinsic joint elasticity. Changing stiffness will have minor effects on F_{max} if other parameters hold unchanged. This result well agrees with the experiment testing with KUKA robots reported in Ref. [25] and MIT Cheetah in Ref. [62].
(2) In contrast, F_{max} of the VSL is considerably affected by the stiffness of the compliant link even if there are no external

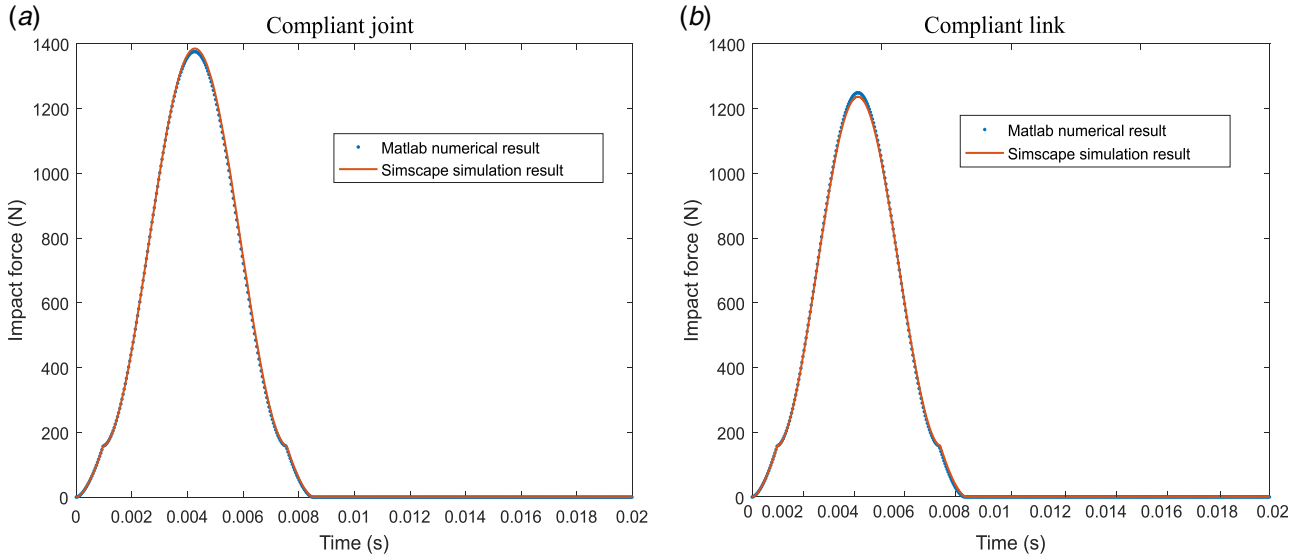

Fig. 4 Validation of the models of the pHRI systems with the CL design and the CJ design

torques applied to the motor. For instance, R_f of the VSL can be up to 57.1% at $v_0 = 3$ m/s. The observation indicates that reducing the stiffness of the compliant link may effectively lower F_{max} of the VSL.

(3) In general, VSJ designs produce a larger F_{max} than VSL designs for each impact velocity. When the lateral stiffness is small (compliant arms), this difference is quite noticeable. However, as the lateral stiffness increases, there is no difference between these two designs. This is because both designs can be regarded as equivalent to the case of a rigid link with a rigid pin joint. The observation is held true for various impact velocities.

Second, we study the case of a constant motor torque applied during the impact process, i.e., $\tau_m \neq 0$. Figures 6(*c*) and 6(*d*) plot $F_{max}(k_l)$ of the VSJ and VSL given various constant torque $\tau_m \in [0, 5]$ N.m. In addition to those observations listed above, two new findings are summarized in the following:

(1) The profile of F_{max} is close to a sigmoid function for both the VSJ and VSL designs. In other words, F_{max} has a sharp "step" change given a certain range of lateral stiffness variation but it is saturated from both sides.

(2) While the VSJ has a slight variation of F_{max}, the magnitude of the variation is much smaller than that of the VSL. For instance, R_f of the VSJ is increased by 4.2% if a constant torque of 5 N.m is applied by the motor. However, the maximum impact force reduction ratio R_f of the VSJ is as high as 39.2% given the same parameters.

It is worth noting that the variation of F_{max} is prominent merely at a certain range of lateral stiffness. In other words, changing the lateral stiffness may not necessarily reduce/increase F_{max} if the stiffness variation is out of the critical range. The prominent variation of F_{max} depends on not only the variation of the lateral stiffness but also on its critical range. This is important for engineers in the design process and will be explored later in more detail.

Next, we take a look at the effects of mass property parameters: the mass ratio R_m and end-effector mass m_e on these plots. Here, we set $\tau_m = 0$. Figures 7(*a*) and 7(*b*) compare $F_{max}(k_l)$ of VSJ and VSL for various R_m. Figures 7(*c*) and 7(*d*) show $F_{max}(k_l)$ given various m_e for VSJ and VSL. In addition to the similar trends as those in Fig. 6, two other findings are summarized in the following.

(1) Without motor torques, the effect of k_l on F_{max} can be almost neglected for the VSJ given various sets of design parameters

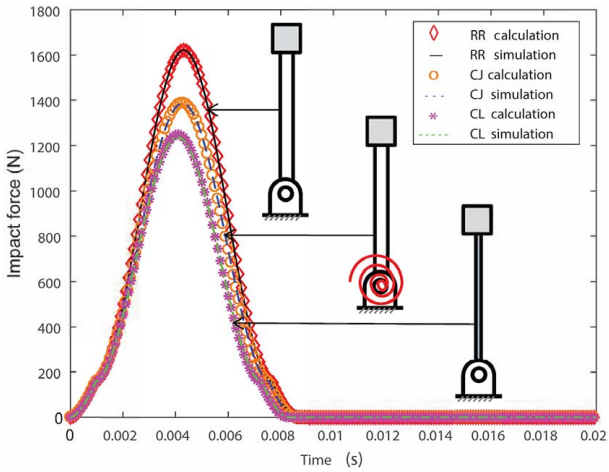

Fig. 5 Validation and comparison of the models of the pHRI systems with the CL design, the CJ design, and the RR design

of R_m and m_e. However, F_{max} of the VSL is noticeably affected by k_l.

(2) Larger R_m or m_e produces larger F_{max} for both the VSJ and VSL. This well agrees with our intuition because larger R_m or m_e generates larger equivalent kinetic energy resulting larger impact force at the end-effector, given all other parameters the same.

4.2 Advantages of the Compliant Link Design. By comparing the performance of the CJ and CL designs, we observed that the link compliance has a better performance in terms of reducing F_{max} for pHRI. We summarized the advantages of the CL design in the following:

(1) The CL design generally produces a smaller F_{max} when compared with that of the CJ design, given the same parameters and lateral stiffness. When lateral stiffness is very large (close to rigid link), there is no difference between CJ and CL designs in terms of maximum impact force. This implies that CL designs are always better than or the same as CJ designs.

(2) Without a motor torque, i.e., free impact, F_{max} is negligibly affected by k_l for the VSJ, but it is considerably affected

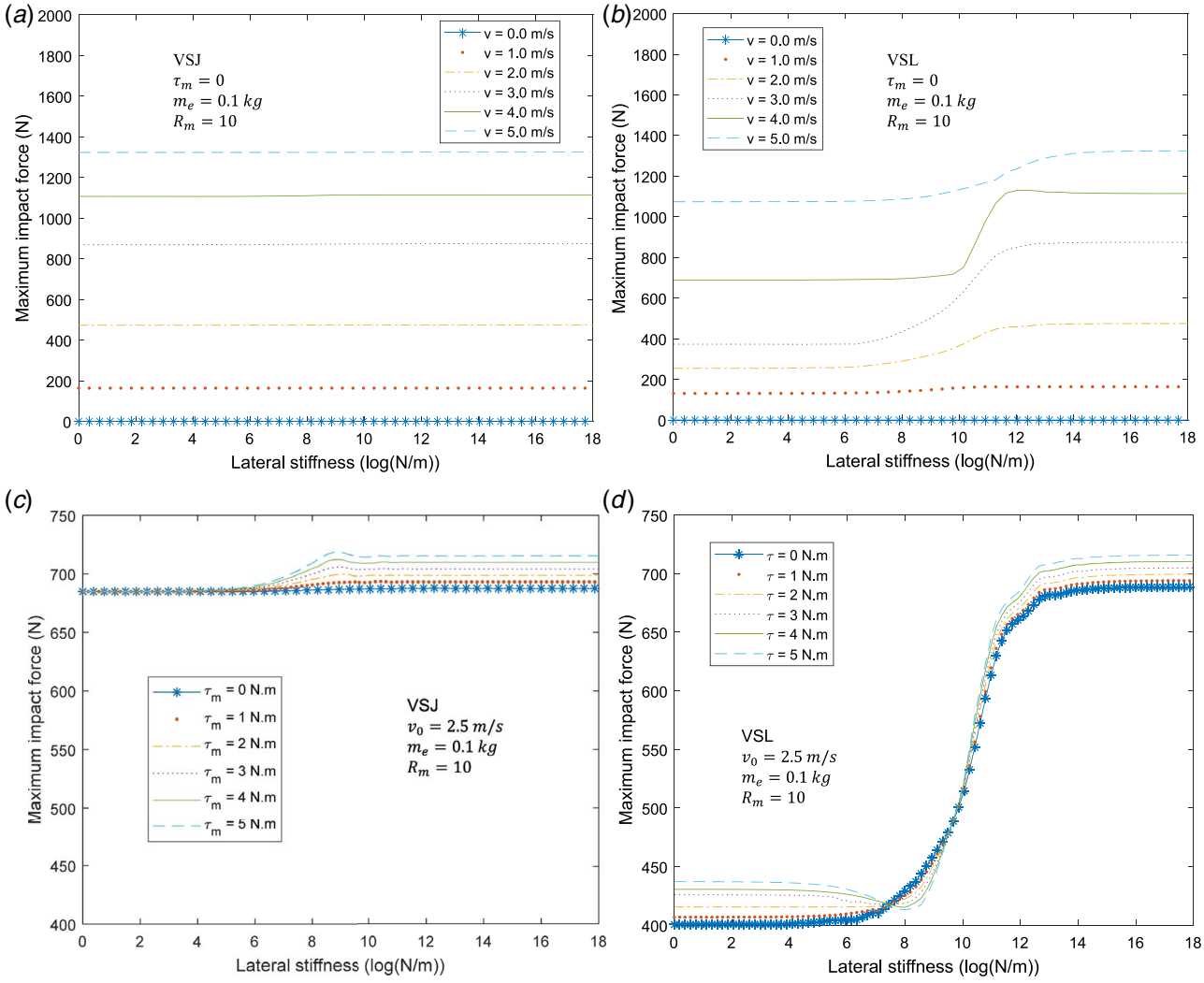

Fig. 6 Comparison of the VSJ with the VSL in terms of maximum impact force F_{max} versus lateral stiffness k_l, given various impact velocities and motor torques: (*a*) the VSJ given various impact velocities, (*b*) the VSL various impact velocities, (*c*) the VSJ given various motor torques, and (*d*) the VSL given various motor torques

by k_l for the VSL with the same other parameters. The observation holds true for various v_0, R_m, and m_e.

(3) With active motor torques, R_f of the VSJ is considerably smaller than that of the VSL.

With these observations, we believe it is possible to effectively reduce F_{max} by reducing k_l for the CL design, no matter whether there is motor torque or not.

Note that we also found the CL design permits a higher bandwidth compared with the CJ design [40]. Therefore, in addition to the benefits of the impact force reduction, the CL design may permit a quicker time response with a smaller settling time than that of the CJ design.

While we believe the proposed method has many potential applications in light-weight robots, especially in the application of low-speed physical human–robot interactions, it is worth mentioning that the method may not apply to highly dynamic systems or heavy inertia robots where the impact velocity and inertia are dominated factors to affect the magnitude of the impact force.

5 Conclusions

This work studies the effects of mechanical compliance on the safety of physical human–robot interaction (pHRI). Theoretical models of the pHRI system with a CJ or CL are developed and validated by simulations. Key conclusions are summarized in the following. The maximum impact force is generally affected by the mechanical compliance for both the CJ and CL designs. However, tuning the stiffness of joints or links may not necessarily reduce/increase the maximum impact force if the stiffness variation is not within a certain range.

Given equivalent lateral stiffness and mass properties parameters, CL designs generally outperform CJ designs in the sense of reducing the maximum impact force. For the case study in the article, the maximum impact force of the CL design is 12.9% less than the CJ design. While the maximum impact force reduction is limited for the CJ design, especially without a motor torque, it is prominent for the CL design. For instance, the CJ design leads to a maximum impact force reduction of 4.2% while the CL design reaches a maximum impact force reduction of 39.2% given the same parameters with an active motor torque of 5 Nm. For the case of free impact (zero motor torque), the CJ design barely achieves impact force reduction due to the decoupling effects, while the CL design can still reduce the maximum impact force by up to 57.1%. The results indicate that the CL design has the potential to reduce the maximum impact force more effectively. This study theoretically demonstrates that the CL design is a promising alternative approach and potentially outperforms the CJ designs in addressing safety in pHRI.

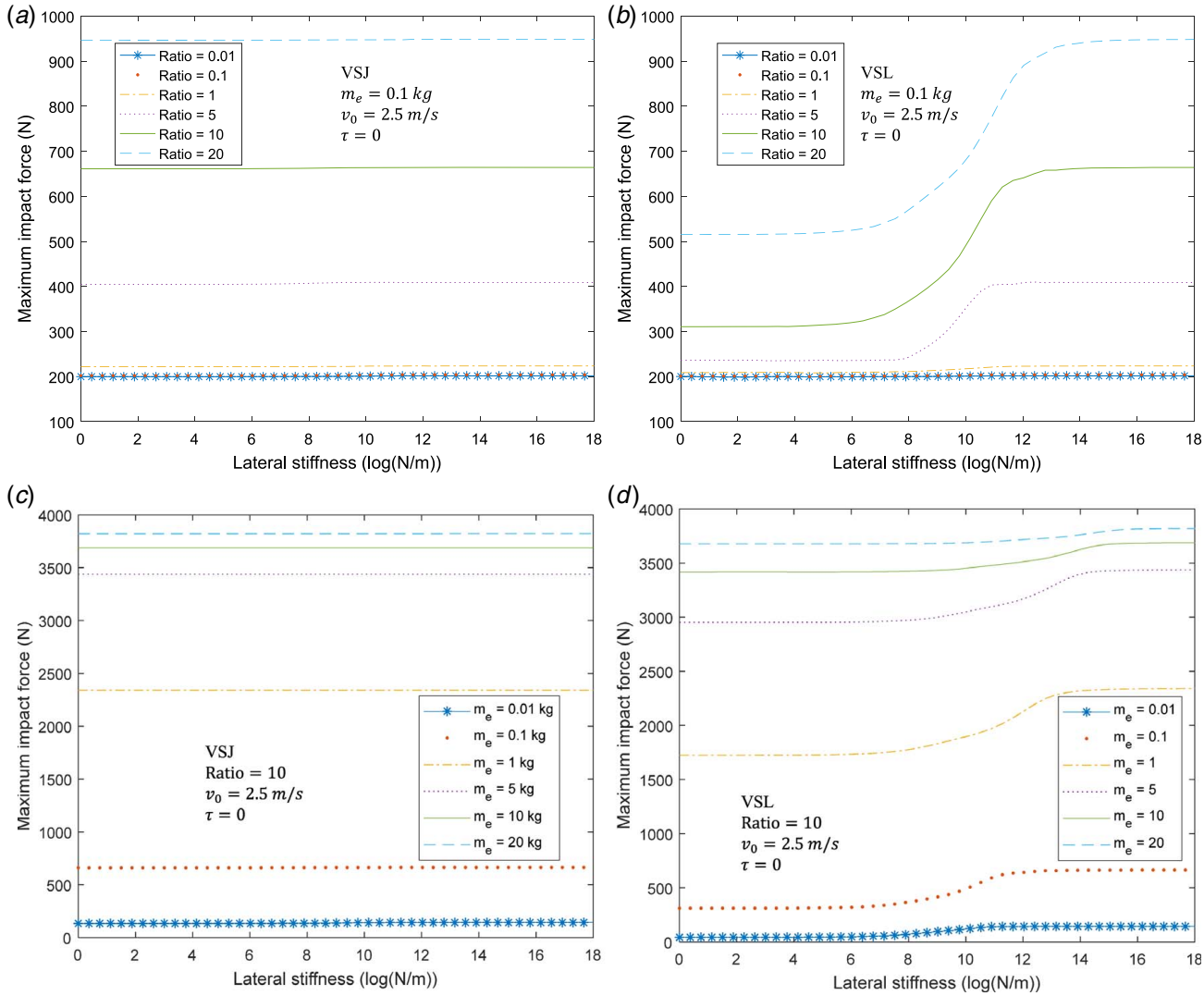

Fig. 7 Comparison of the VSJ with the VSL in terms of maximum impact force F_{max} versus lateral stiffness k_l, given various mass ratios and end-effector mass: (*a*) the VSJ given various mass ratios, (*b*) the VSL given various mass ratios, (*c*) the VSJ given various end-effector mass, and (*d*) the VSL given various end-effector mass

Acknowledgment

This material is based upon the work supported by the National Science Foundation under Grant No: CMMI-1637656. Any opinions, findings, and conclusions or recommendations expressed in this material are those of the author(s) and do not necessarily reflect the views of the funding agencies.

References

[1] Müller, R., Vette, M., and Scholer, M., 2014, "Inspector Robot–A New Collaborative Testing System Designed for the Automotive Final Assembly Line," Assembly Autom., **34**(4), pp. 370–378.

[2] Kragic, D., Marayong, P., Li, M., Okamura, A. M., and Hager, G. D., 2005, "Human-Machine Collaborative Systems for Microsurgical Applications," Int. J. Robot. Res., **24**(9), pp. 731–741.

[3] Bauer, A., Wollherr, D., and Buss, M., 2008, "Human–Robot Collaboration: A Survey," Int. J. Humanoid Rob., **5**(01), pp. 47–66.

[4] Albu-Schäffer, A., Haddadin, S., Ott, C., Stemmer, A., Wimböck, T., and Hirzinger, G., 2007, "The DLR Lightweight Robot: Design and Control Concepts for Robots in Human Environments," Ind. Rob.: An Int. J., **34**(5), pp. 376–385.

[5] Vanderborght, B., Albu-Schäffer, A., Bicchi, A., Burdet, E., Caldwell, D. G., Carloni, R., Catalano, M., Eiberger, O., Friedl, W., Ganesh, G., Garabini, M., Grebenstein, M., Grioli, G., Haddadin, S., Hoppner, H., Jafari, A., Laffranchi, M., Lefeber, D., Petit, F., Stramigioli, S., Tsagarakis, N., Van Damme, M., Van Ham, R., Visser, L. C., and Wolf, S., 2013, "Variable Impedance Actuators: A Review," Rob. Auton. Syst., **61**(12), pp. 1601–1614.

[6] Ficuciello, F., Villani, L., and Siciliano, B., 2015, "Variable Impedance Control of Redundant Manipulators for Intuitive Human–Robot Physical Interaction," IEEE Trans. Rob., **31**(4), pp. 850–863.

[7] Howe, R. D., and Cutkosky, M. R., 1993, "Dynamic Tactile Sensing: Perception of Fine Surface Features With Stress Rate Sensing," IEEE Trans. Rob. Autom., **9**(2), pp. 140–151.

[8] Feddema, J. T., and Novak, J. L., 1994, "Whole Arm Obstacle Avoidance for Teleoperated Robots," IEEE International Conference on Robotics and Automation, San Diego, CA, May 8–13, pp. 3303–3309.

[9] Lumelsky, V. J., and Cheung, E., 1993, "Real-Time Collision Avoidance in Teleoperated Whole-Sensitive Robot Arm Manipulators," IEEE Trans. Syst. Man Cybern., **23**(1), pp. 194–203.

[10] Heinzmann, J., and Zelinsky, A., 2003, "Quantitative Safety Guarantees for Physical Human-Robot Interaction," Int. J. Robot. Res., **22**(7–8), pp. 479–504.

[11] Najmaei, N., and Kermani, M. R., 2011, "Applications of Artificial Intelligence in Safe Human–Robot Interactions," IEEE Trans. Syst. Man Cybern., Part B (Cybernetics), **41**(2), pp. 448–459.

[12] Kong, K., Bae, J., and Tomizuka, M., 2009, "Control of Rotary Series Elastic Actuator for Ideal Force-Mode Actuation in Human–Robot Interaction Applications," IEEE/ASME Trans. Mechatron., **14**(1), pp. 105–118.

[13] Avanzini, G. B., Ceriani, N. M., Zanchettin, A. M., Rocco, P., and Bascetta, L., 2014, "Safety Control of Industrial Robots Based on a Distributed Distance Sensor," IEEE Trans. Control Syst. Technol., **22**(6), pp. 2127–2140.

[14] Bicchi, A., Tonietti, G., and Piaggio, E., 2002, "Design, Realization and Control of Soft Robot Arms for Intrinsically Safe Interaction With Humans," Proceedings of the IARP/RAS Workshop on Technical Challenges for Dependable Robots in Human Environments, Toulouse, France, Oct. 7–8, pp. 79–87.

[15] Bicchi, A., and Tonietti, G., 2004, "Fast and" Soft-Arm" Tactics [Robot Arm Design]," IEEE Robot. Automat. Mag., **11**(2), pp. 22–33.

[16] Bicchi, A., Bavaro, M., Boccadamo, G., De Carli, D., Filippini, R., Grioli, G., Piccigallo, M., Rosi, A., Schiavi, R., Sen, S., and Tonietti, G., 2008, "Physical Human-Robot Interaction: Dependability, Safety, and Performance," 10th IEEE International Workshop on Advanced Motion Control, Trento, Italy, Mar. 26–28, pp. 9–14.
[17] Tonietti, G., Schiavi, R., and Bicchi, A., 2006, "Optimal Mechanical/Control Design for Safe and Fast Robotics," *Experimental Robotics IX*, Springer, New York, pp. 311–320.
[18] Tonietti, G., Schiavi, R., and Bicchi, A., 2005, "Design and Control of a Variable Stiffness Actuator for Safe and Fast Physical Human/Robot Interaction," Proceedings of the 2005 IEEE International Conference on Robotics and Automation, Barcelona, Spain, Apr. 18–22, pp. 526–531.
[19] Schiavi, R., Grioli, G., Sen, S., and Bicchi, A., 2008, "Vsa-II: A Novel Prototype of Variable Stiffness Actuator for Safe and Performing Robots Interacting With Humans," IEEE International Conference on Robotics and Automation, Pasadena, CA, May 19–23, pp. 2171–2176.
[20] Chen, L., Garabini, M., Laffranchi, M., Kashiri, N., Tsagarakis, N. G., Bicchi, A., and Caldwell, D. G., 2013, "Optimal Control for Maximizing Velocity of the ™ Compliant Actuator," IEEE International Conference on Robotics and Automation, Karlsruhe, Germany, May 6–10, pp. 516–522.
[21] Wolf, S., and Hirzinger, G., 2008, "A New Variable Stiffness Design: Matching Requirements of the Next Robot Generation," IEEE International Conference on Robotics and Automation, Pasadena, CA, May 19–23, pp. 1741–1746.
[22] Wolf, S., Eiberger, O., and Hirzinger, G., 2011, "The Dlr Fsj: Energy Based Design of a Variable Stiffness Joint," IEEE International Conference on Robotics and Automation, Shanghai, China, May 9–13, pp. 5082–5089.
[23] Friedl, W., Höppner, H., Petit, F., and Hirzinger, G., 2011, "Wrist and Forearm Rotation of the Dlr Hand Arm System: Mechanical Design, Shape Analysis and Experimental Validation," IEEE/RSJ International Conference on Intelligent Robots and Systems, San Francisco, CA, Sept. 25–30, pp. 1836–1842.
[24] Zinn, M., Roth, B., Khatib, O., and Salisbury, J. K., 2004, "A New Actuation Approach for Human Friendly Robot Design," Int. J. Rob. Res., **23**(4–5), pp. 379–398.
[25] Haddadin, S., Albu-Schäffer, A., and Hirzinger, G., 2009, "Requirements for Safe Robots: Measurements, Analysis and New Insights," Int. J. Rob. Res., **28**(1112), pp. 1507–1527.
[26] Haddadin, S., Albu-Schäffer, A., Eiberger, O., and Hirzinger, G., 2010, "New Insights Concerning Intrinsic Joint Elasticity for Safety," IEEE/RSJ International Conference on Intelligent Robots and Systems, Taipei, Taiwan, Oct. 18–22, pp. 2181–2187.
[27] Migliore, S. A., Brown, E. A., and DeWeerth, S. P., 2005, "Biologically Inspired Joint Stiffness Control," Proceedings of the 2005 IEEE International Conference on Robotics and Automation, Barcelona, Spain, Apr. 18–22, pp. 4508–4513.
[28] Koganezawa, K., 2005, "Mechanical Stiffness Control for Antagonistically Driven Joints," IEEE/RSJ International Conference on Intelligent Robots and Systems, Edmonton, Alta., Canada, Aug. 2–6, pp. 1544–1551.
[29] Pratt, G. A., and Williamson, M. M., 1995, "Series Elastic Actuators," IEEE/RSJ International Conference on Intelligent Robots and Systems, Pittsburgh, PA, Aug. 5–9, pp. 399–406.
[30] Carpino, G., Accoto, D., Sergi, F., Tagliamonte, N. L., and Guglielmelli, E., 2012, "A Novel Compact Torsional Spring for Series Elastic Actuators for Assistive Wearable Robots," ASME J. Mech. Des., **134**(12), p. 121002.
[31] Wu, Y.-S., and Lan, C.-C., 2014, "Linear Variable-Stiffness Mechanisms Based on Preloaded Curved Beams," ASME J. Mech. Des., **136**(12), p. 122302.
[32] Park, J.-J., Kim, B.-S., Song, J.-B., and Kim, H.-S., 2007, "Safe Link Mechanism Based on Passive Compliance for Safe Human-Robot Collision," IEEE International Conference on Robotics and Automation, Roma, Italy, Apr. 10–14, pp. 1152–1157.
[33] Park, J.-J., Kim, B.-S., Song, J.-B., and Kim, H.-S., 2008, "Safe Link Mechanism Based on Nonlinear Stiffness for Collision Safety," Mech. Mach. Theory, **43**(10), pp. 1332–1348.
[34] Park, J.-J., and Song, J.-B., 2010, "A Nonlinear Stiffness Safe Joint Mechanism Design for Human Robot Interaction," ASME J. Mech. Des., **132**(6), p. 061005.
[35] López-Martínez, J., Blanco-Claraco, J. L., García-Vallejo, D., and Giménez-Fernández, A., 2015, "Design and Analysis of a Flexible Linkage for Robot Safe Operation in Collaborative Scenarios," Mech. Mach. Theory, **92**, pp. 1–16.
[36] Zhang, M., Laliberté, T., and Gosselin, C., 2016, "Force Capabilities of Two-Degree-of-Freedom Serial Robots Equipped With Passive Isotropic Force Limiters," ASME J. Mech. Rob., **8**(5), p. 051002.
[37] Stilli, A., Wurdemann, H. A., and Althoefer, K., 2014, "Shrinkable, Stiffness-Controllable Soft Manipulator Based on a Bio-Inspired Antagonistic Actuation Principle," 2014 IEEE/RSJ International Conference on Intelligent Robots and Systems, Chicago, IL, Sept. 14–18, pp. 2476–2481.
[38] Stilli, A., Wurdemann, H. A., and Althoefer, K., 2017, "A Novel Concept for Safe, Stiffness-Controllable Robot Links," Soft Rob., **4**(1), pp. 16–22.
[39] She, Y., Su, H.-J., and Hurd, C. J., 2015, "Shape Optimization of 2D Compliant Links for Design of Inherently Safe Robots," ASME 2015 International Design Engineering Technical Conferences and Computers and Information in Engineering Conference, Boston, MA, Aug. 2–5, Paper No. DETC2015-46622.
[40] She, Y., Su, H.-J., Meng, D., Song, S., and Wang, J., 2018, "Design and Modeling of a Compliant Link for Inherently Safe Corobots," ASME J. Mech. Rob., **10**(1), p. 011001.
[41] She, Y., Su, H.-J., Lai, C., and Meng, D., 2016, "Design and Prototype of a Tunable Stiffness Arm for Safe Human-Robot Interaction," ASME 2016 International Design Engineering Technical Conferences and Computers and Information in Engineering Conference, Charlotte, NC, Aug. 21–24, Paper No. DETC2016-59523.
[42] She, Y., Su, H.-J., Meng, D., and Lai, C., 2019, "Design and Modeling of a Continuously Tunable Stiffness Arm for Safe Physical Human-Robot Interaction," ASME J. Mech. Rob., **12**(1), pp. 1–15.
[43] She, Y.,2018, "Compliant Robotic Arms for Inherently Safe Physical Human–Robot Interaction". Ph.D. thesis, The Ohio State University, Columbus, OH.
[44] Laffranchi, M., Tsagarakis, N. G., and Caldwell, D. G., 2010, "A Variable Physical Damping Actuator (VPDA) for Compliant Robotic Joints," IEEE International Conference on Robotics and Automation, Anchorage, AK, May 3–7, pp. 1668–1674.
[45] Laffranchi, M., Tsagarakis, N. G., and Caldwell, D. G., 2013, "Analysis and Development of a Semiactive Damper for Compliant Actuation Systems," IEEE/ASME Trans. Mechatron., **18**(2), pp. 744–753.
[46] Chew, C.-M., Hong, G.-S., and Zhou, W., 20042004, "Series Damper Actuator: A Novel Force/Torque Control Actuator," Fourth IEEE/RAS International Conference on Humanoid Robots, Santa Monica, CA, Nov. 10–12, pp. 533–546.
[47] Fauteux, P., Lauria, M., Heintz, B., and Michaud, F., 2010, "Dual-Differential Rheological Actuator for High-Performance Physical Robotic Interaction," IEEE Trans. Rob., **26**(4), pp. 607–618.
[48] Kostamo, E., Focchi, M., Guglielmino, E., Kostamo, J., Semini, C., Buchli, J., Pietola, M., and Caldwell, D., 2014, "Magnetorheologically Damped Compliant Foot for Legged Robotic Application," ASME J. Mech. Des., **136**(2), p. 021003.
[49] Sodano, H. A., Bae, J.-S., Inman, D. J., and Belvin, W. K., 2006, "Improved Concept and Model of Eddy Current Damper," ASME J. Vib. Acoust., **128**(3), pp. 294–302.
[50] Hou, C.-Y., 2008, "Fluid Dynamics and Behavior of Nonlinear Viscous Fluid Dampers," J. Struct. Eng., **134**(1), pp. 56–63.
[51] Versace, J., 1971, A Review of the Severity Index, Technical Report, SAE Technical Paper.
[52] Gao, D., and Wampler, C. W., 2009, "Head Injury Criterion," IEEE Rob. Autom. Mag., **16**(4), pp. 71–74.
[53] Haddadin, S., Albu-Schaffer, A., Frommberger, M., Rossmann, J., and Hirzinger, G., 2009, "The "DLR Crash Report": Towards a Standard Crash-Testing Protocol for Robot Safety-Part I: Results," IEEE International Conference on Robotics and Automation, Kobe, Japan, May 12–17, pp. 272–279.
[54] ISO10218-1:2006, 2006, *Robots for Industrial Environments - Safety Requirements. Part I: Robot*, International Organization for Standarization.
[55] Melvin, J.,1980, Human Tolerance to Impact Conditions as Related to Motor Vehicle Design, SAE Report J885, April 1980.
[56] Framework, E., 2003, "Improved Frontal Impact Protection Through a World Frontal Impact dummy," Project No. GRD1 1999, 10559.
[57] Park, J.-J., Haddadin, S., Song, J.-B., and Albu-Schäffer, A., 2011, "Designing Optimally Safe Robot Surface Properties for Minimizing the Stress Characteristics of Human-Robot Collisions," IEEE International Conference on Robotics and Automation, Shanghai, China, May 9–13, pp. 5413–5420.
[58] She, Y., Meng, D., Cui, J., and Su, H.-J., 2017, "On the Impact Force of Human-Robot Interaction: Joint Compliance vs. Link Compliance," 2017 IEEE International Conference on Robotics and Automation, Marina Bay, Singapore, May 29–June 3, pp. 6718–6723.
[59] Johnson, K. L., and Johnson, K. L., 1987, *Contact Mechanics*, Cambridge University Press, Cambridge, UK.
[60] López-Martínez, J., García-Vallejo, D., Giménez-Fernández, A., and Torres-Moreno, J., 2014, "A Flexible Multibody Model of a Safety Robot Arm for Experimental Validation and Analysis of Design Parameters," ASME J. Comput. Nonlinear Dyn., **9**(1), p. 011003.
[61] Book, W. J., 1984, "Recursive Lagrangian Dynamics of Flexible Manipulator Arms," Int. J. Rob. Res., **3**(3), pp. 87–101.
[62] Wensing, P. M., Wang, A., Seok, S., Otten, D., Lang, J., and Kim, S., 2017, "Proprioceptive Actuator Design in the MIT Cheetah: Impact Mitigation and High-Bandwidth Physical Interaction for Dynamic Legged Robots," IEEE Trans. Rob., **33**(3), pp. 509–522.